



ARTICLE

Research on Image Motion Compensation of an Airborne Camera with a Focal Plane Charge-Coupled Device Camera and an Analysis of Image Motion

Hang Ren^{1,3} and TaoTao Hu^{2,*}

The imaging quality of a target is dramatically influenced by image motion (IM), which results from the relative movement between a charge-coupled device (CCD) camera and an aircraft during the exposure time. Therefore, it is quite necessary to produce appropriate systems to compensate for this kind of movement and achieve high-quality, real-time imaging. The image motion velocity should be precisely calculated to compensate for the image motion as much as possible. In the paper, several methods were introduced to calculate the image motion velocity by using coordinate transformation, which deduced the image motion value of a given point by considering the difference before and after the gesture angles and position changes. Furthermore, both a theoretical and a mechanical image motion compensation (IMC) method were analyzed. A three-axis stable platform was assembled between the camera system and the unmanned aircraft. The IM caused by variation in the airplane gesture angles, including the pitch angle, yaw angle and roll angle, could be compensated by the reverse rotation of the stable platform in the corresponding axis. Similarly, the IM caused by the aircraft's continuing flight could be compensated by the reverse rotation in the pitch axis. The residual errors of the IMC of the camera from the aircraft navigation were analyzed and calculated in detail. The residual errors of the image points were less than one third of the diameter of a CCD pixel, which demonstrates that the IMC system satisfied the imaging system.

Keywords: Focal Plane CCD Camera, Image Motion, Image Motion Compensation, Residual Error, Coordinate Transformation.

1. INTRODUCTION

When an aerial camera takes an aerial photograph, due to the high-speed flight of the aircraft, there is relative motion between the camera and the target during the exposure time, which causes the image motion of the target on the focal plane to change, producing image motion. The image

motion moves the images of different objects relative to each other, causing the image to degrade. The image appears to have trailing, blurred edges [1–3], grayscale distortion, and reduced contrast and resolution. The reasons for this displacement are divided into the forward image motion caused by the forward flight of the aircraft, the random image motion caused by changes in the attitude (such as pitch, yaw, and roll) of the aircraft, the motion of the aircraft components (such as propellers and engine blocks) and camera platforms, the vibration of the camera itself due to operation or impact and the image vibration caused by the fluctuation in the air flow. In a vertically photographing aerial camera, the amount of forward image motion is one order of magnitude higher than that of other image motions, so the main consideration for this type of camera is to compensate for forward image motion [4–7]. Although the image degradation caused by image motion can be restored using image processing methods according

¹Changchun Institute of Optics, Fine Mechanics and Physics, Chinese Academy of Sciences, Changchun, 130033, China

²School of Physics, Northeast Normal University, ChangChun, 130024, China

³Key Laboratory of Airborne Optical Imaging and Measurement, Changchun Institute of Optics, Fine Mechanics and Physics, Chinese Academy of Sciences, Changchun, 130033, China

*Author to whom correspondence should be addressed.

Email: hutt262@nenu.edu.cn

Received: 15 December 2021

Accepted: 18 December 2021

of the system. This method is a relatively mature method that uses the basic law of light propagation to accurately calculate the imaging conditions when the optical system changes. For static optical systems, ray tracing is a classic and effective method. However, there are limitations to the changing of the optical system. Since vibration is a function of time, if one wants to find the displacement of the image point at each moment, one needs to trace the light at every moment of the vibration. This approach results in a large number of calculations [27, 28].

The coordinate transformation method is a computationally simple image motion method that has been successfully applied to the calculation of image motion compensation for optical imaging by remote sensors. This method analyzes in detail the coordinate transformation equations from the ground to the image surface of the optical imaging remote sensor and accurately calculates the movement of the scene caused by the rotation of the earth and the orbit of the spacecraft on the image plane [29, 30].

The orthogonal projection analysis method considers main factors, ignores secondary factors, considers the independent action components of each factor, and ignores the coupling action components. This method has a simple expression and is easy to calculate; furthermore, it is easy to use for engineering, but a certain image motion error remains after compensation, and it is difficult to calculate the amount of image motion in complex optical systems with this method.

2.2. Method of Coordinate Transformation

The principle of the coordinate transformation method is that the rotation of the coordinate system is equivalent to the attitude transformation of the camera, and the amount of image motion and the speed of the image motion are obtained by the matrix relationship between different coordinate values of the image plane before and after the camera attitude transformation at the same point on the ground. This method is intuitive and simple.

The method of representing an n -dimensional subvector with an $(n+1)$ -dimensional subvector is called "homogeneous coordinate representation." For example, a rectangular coordinate (x, y, z) of a point P in a three-dimensional space is expressed as a homogeneous coordinate, which is (W_x, W_y, W_z, W) . The relationship of this coordinate with ordinary rectangular coordinates can be converted by the following formula [31, 32]:

$$x = W_x/W, y = W_y/W, z = W_z/W \quad (1)$$

The origin of the graph is centered (zoomed out).

$$\begin{bmatrix} S_x & 0 & 0 & 0 \\ 0 & S_y & 0 & 0 \\ 0 & 0 & S_z & 0 \\ 0 & 0 & 0 & 1 \end{bmatrix} \begin{bmatrix} x \\ y \\ z \\ 1 \end{bmatrix} = \begin{bmatrix} S_x x \\ S_y y \\ S_z z \\ 1 \end{bmatrix} = \begin{bmatrix} x' \\ y' \\ z' \\ 1 \end{bmatrix} \quad (2)$$

The graph is centered around the origin and zooms in (zooms out) S_x, S_y, S_z times in the $x, y,$ and z directions, respectively. A graphical translation is shown

$$\begin{bmatrix} 1 & 0 & 0 & e \\ 0 & 1 & 0 & f \\ 0 & 0 & 1 & g \\ 0 & 0 & 0 & 1 \end{bmatrix} \begin{bmatrix} x \\ y \\ z \\ 1 \end{bmatrix} = \begin{bmatrix} x+e \\ y+f \\ z+g \\ 1 \end{bmatrix} = \begin{bmatrix} x' \\ y' \\ z' \\ 1 \end{bmatrix} \quad (3)$$

The graphic moves $e, f,$ and g in the $x, y,$ and z directions, respectively, or the coordinate system origin moves relative to the graphic in the $x, y,$ and z directions by $-e, -f,$ and $-g,$ respectively [15].

The graphics rotate around the x axis:

$$\begin{bmatrix} 1 & 0 & 0 & 0 \\ 0 & \cos \theta & -\sin \theta & 0 \\ 0 & \sin \theta & \cos \theta & 0 \\ 0 & 0 & 0 & 1 \end{bmatrix} \begin{bmatrix} x \\ y \\ z \\ 1 \end{bmatrix} = \begin{bmatrix} x \\ \cos \theta y - \sin \theta z \\ \sin \theta y + \cos \theta z \\ 1 \end{bmatrix} = \begin{bmatrix} x' \\ y' \\ z' \\ 1 \end{bmatrix} \quad (4)$$

This equation means that

$$x' = x; \quad y' = \cos \theta y - \sin \theta z; \quad z' = \sin \theta y + \cos \theta z \quad (5)$$

This phenomenon can also be viewed as the result of the coordinate system rotating by an angle of " $-\theta$ " around the x axis relative to the pattern. The graphics rotate around the y axis.

$$\begin{bmatrix} \cos \theta & 0 & \sin \theta & 0 \\ 0 & 1 & 0 & 0 \\ -\sin \theta & 0 & \cos \theta & 0 \\ 0 & 0 & 0 & 1 \end{bmatrix} \begin{bmatrix} x \\ y \\ z \\ 1 \end{bmatrix} = \begin{bmatrix} \cos \theta x + \sin \theta z \\ y \\ -\sin \theta x + \cos \theta z \\ 1 \end{bmatrix} = \begin{bmatrix} x' \\ y' \\ z' \\ 1 \end{bmatrix} \quad (6)$$

This equation means that

$$x' = \cos \theta x + \sin \theta z, \quad y' = y, \quad z' = -\sin \theta x + \cos \theta z \quad (7)$$

This phenomenon can also be viewed as the result of the coordinate system rotating by an angle of " $-\theta$ " around the y axis relative to the pattern. The graphics rotate around the z axis.

$$\begin{bmatrix} \cos \theta & -\sin \theta & 0 & 0 \\ \sin \theta & \cos \theta & 0 & 0 \\ 0 & 0 & 1 & 0 \\ 0 & 0 & 0 & 1 \end{bmatrix} \begin{bmatrix} x \\ y \\ z \\ 1 \end{bmatrix} = \begin{bmatrix} \cos \theta x - \sin \theta y \\ \sin \theta x + \cos \theta y \\ z \\ 1 \end{bmatrix} = \begin{bmatrix} x' \\ y' \\ z' \\ 1 \end{bmatrix} \quad (8)$$

This equation means that $x' = \cos \theta x - \sin \theta y$, $y' = \sin \theta x + \cos \theta y$, $z' = z$.

In this case, this phenomenon can also be regarded as the result of the coordinate system rotating by an angle “ $-\theta$ ” around the z axis with respect to the figure. An object coordinate transformation on objective lens imaging is shown.

$$\begin{bmatrix} -f'/z & 0 & 0 & 0 \\ 0 & -f'/z & 0 & 0 \\ 0 & 0 & (f'/z)^2 & 0 \\ 0 & 0 & 0 & 1 \end{bmatrix} \begin{bmatrix} x \\ y \\ z \\ 1 \end{bmatrix} = \begin{bmatrix} -f'x/z \\ -f'y/z \\ (f'/z)^2 z \\ 1 \end{bmatrix} = \begin{bmatrix} x' \\ y' \\ z' \\ 1 \end{bmatrix} \quad (9)$$

Here, f' is the objective lens focal length.

The above matrices only list transformations wherein the optical axis coincides with the z -axis, and a transformation matrix in which the optical axis coincides with the x -axis or y -axis is not difficult to write. The general transformation matrix of three-dimensional homogeneous coordinates can be expressed in the following form:

$$T = \begin{bmatrix} a & b & c & p \\ d & e & f & q \\ h & i & j & r \\ l & m & n & s \end{bmatrix} \Rightarrow \begin{bmatrix} 3 & & & \\ & 3 & & \\ & & 1 & \\ & & & 3 \end{bmatrix} \quad (10)$$

Divide the 4×4 transform matrix into four blocks, with a 3×3 matrix producing proportional relations, miscuts and rotations:

- a 3×1 matrix produces a translation;
- a 1×3 matrix produces perspective transformations; and
- the 1×1 matrix produces all the scale transformations.

2.3. Selection of a Coordinate System and the Definition of an Attitude Angle

2.3.1. Definition of a Coordinate System

(a) Track the coordinate system G (G_1, G_2, G_3).

The origin is usually fixed at the center of gravity of the aircraft. The G_1 axis is in the direction of the track velocity. The G_3 axis is in the vertical plane containing the G_1 axis, perpendicular to the G_1 axis and pointing downwards, and G_2 is perpendicular to the G_1G_3 plane and pointing to the right.

(b) The aircraft is involved in the vertical ground coordinate system C (C_1, C_2, C_3).

The origin is usually fixed at the center of gravity of the aircraft. The direction of each axis is the same as G_1, G_2 , and G_3 .

(c) Body coordinate system S (S_1, S_2, S_3).

The origin is usually fixed at the center of gravity of the aircraft. S_1 is the axis that points forward in the aircraft's reference plane.

S_2 , which is also known as the vertical axis and denoted as x , is perpendicular to the aircraft reference plane and points to the right coordinate axis, also commonly referred to as the horizontal axis and denoted as y . S_3 is the coordinate axis that is perpendicular to the vertical axis within the aircraft reference plane, which is also known as the vertical axis and is denoted as z . When the aircraft does not change its attitude, the S -series and the B -series coincide [33–34].

(d) Camera coordinate system B (B_1, B_2, B_3).

The main point of the camera objective lens is the origin of the coordinate system. When the camera is in the spacecraft, there is no installation error or the error is negligible.

Slightly tilted, the camera coordinate system coincides with the body coordinate system.

(e) Image Plane P (P_1, P_2, P_3).

The origin of this coordinate system is at the center of the image plane, and the C system is translated along the C_3 axis f (the focal length of the camera objective lens).

When the scale is reduced by f/H , the P -plane and P_1 and P_2 imaging planes are obtained. M is a ground plane parallel to the $1\ 2\ G\ OG$ plane. The intersection point between the $3\ OS$ axis and the ground plane M is point A . That is, the center point of the image plane corresponds to the ground target point A [35]. As shown in Figure 2.

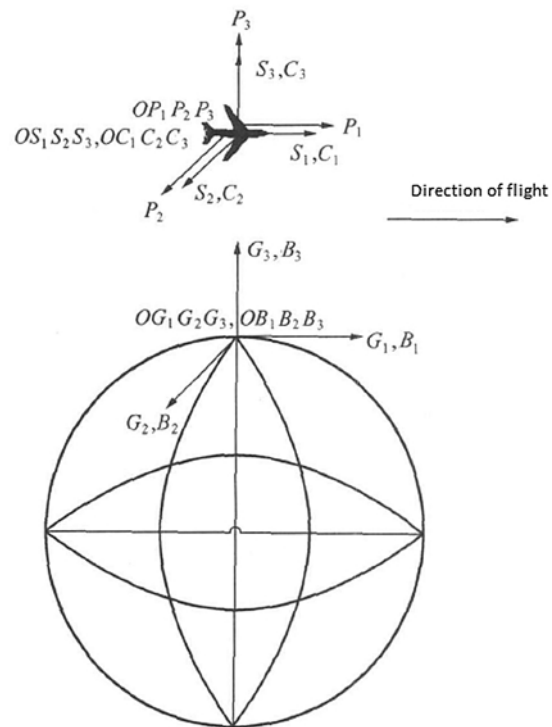


Fig. 2. Definitions of the coordinate systems.

2.3.2. Definition of Aircraft Attitude

The aircraft's three-axis attitude refers to the angle of the aircraft's coordinate axis relative to the plane's implied vertical ground axis including the yaw angle, pitch angle, and roll angle (tilt angle).

(a) Definition of the yaw angle.

The yaw angle is the angle at which the axis of the vertical ground coordinate system and the axis of the axis of the aircraft involved in the plane's rotation coincide with the projection of the vertical axis of the body at the level of the overorigin. Alternatively, the yaw angle is defined as the angle between the projection of the vertical body axis and the B1 axis. When the projection line of the positive half axis of the vertical axis is on the right side of the B1 axis, the yaw angle is positive [36].

(b) Definition of pitch angle.

According to the definition of yaw angle, after turning the B1 axis through the β angle, it is rotated through the angle in the vertical plane.

The B2 angle turns to coincide with the longitudinal axis of the body or the angle between the vertical axis of the body and the horizontal plane.

When the positive half axis of the vertical axis is above the horizontal plane of the origin, θ is positive. By convention, the range of θ is $-(\pi/2) \leq \theta \leq (\pi/2)$.

(c) Definition of the roll angle

After the aircraft's vertical ground coordinate system has been subjected to two rotations of ψ and θ , it is rotated around the vertical axis so that the B2 axis after turning the ψ angle coincides with the horizontal axis of the aircraft or the angle between the vertical axis of the body and the vertical plane passing through the vertical axis. When the positive semi-axis of the vertical axis is to the left of this vertical plane, φ is positive.

(d) Definition of the offset

The offset is determined by the speed of the track and the plane of reference of the aircraft. When the track velocity along the horizontal axis of the body is positive, β is positive [37].

2.3.3. Definitions for Symbols

V —Flight speed of the aircraft (m/s).

H —Aircraft flight altitude (m).

T —Change in the amount of time.

τ —Exposure time.

ψ, θ, φ —Yaw, pitch and roll attitude at the times of the photographs, $\psi = \dot{\psi}t + \psi_0$.

$\theta = \theta_0 + \dot{\theta}t, \quad \varphi = \varphi_0 + \dot{\varphi}t$

$\dot{\psi}, \dot{\theta}, \dot{\varphi}$ —Yaw, pitch, and roll angular velocities when the photograph was taken.

f —Camera lens focal length ().

V_{p1}, V_{p2} —Horizontal and forward image motion speed ($\mu\text{m/s}$) on the camera's surface, respectively.

V_p —Image speed on the camera surface main vector value (mm/s).

m_1, m_2 —The coordinates of the center of the image plane in the track coordinate system.

p_1, p_2 —At the moment of photography, the coordinates $P(p_1, p_2)$ of any point on the camera image plane.

g_1, g_2 —At the moment of photography, the ground photography target corresponding to any point on the camera image surface is in the ground coordinate system position $G(g_1, g_2)$.

L —The distance from the intersection of the extension line of the projection center with the center point of the image plane and the ground plane to the projection center.

L' —The distance between any point on the ground plane and the projection center

2.4. Calculation of the Image Motion of the Vertical Area CCD Array Camera

When the three attitude angles of the aircraft are changed, the corresponding relationship can be established through the transformation process from the position of the ground object in the track coordinate system to the image in the image plane coordinate system. From the position of the feature in the track coordinate system relative to the image in the image coordinate system, the relationship can be established by the transformation process shown in Figure 3.

The transformation process from the ground coordinate system to the image coordinate system can be obtained from the transformation process in Figure 3.

$$p = \begin{pmatrix} p_1 \\ p_2 \\ p_3 \\ 1 \end{pmatrix} = \begin{pmatrix} -\frac{f}{L} & 0 & 0 & 0 \\ 0 & -\frac{f}{L} & 0 & 0 \\ 0 & 0 & \left(\frac{f}{L}\right)^2 & 0 \\ 0 & 0 & 0 & 1 \end{pmatrix} \times \begin{pmatrix} 1 & 0 & 0 & 0 \\ 0 & \cos \varphi & \sin \varphi & 0 \\ 0 & -\sin \varphi & \cos \varphi & 0 \\ 0 & 0 & 0 & 1 \end{pmatrix} \times \begin{pmatrix} \cos \theta & 0 & -\sin \theta & 0 \\ 0 & 1 & 0 & 0 \\ \sin \theta & 0 & \cos \theta & 0 \\ 0 & 0 & 0 & 1 \end{pmatrix} \times \begin{pmatrix} \cos \psi & 0 & -\sin \psi & 0 \\ -\sin \psi & \cos \psi & 1 & 0 \\ 0 & 0 & 1 & 0 \\ 0 & 0 & 0 & 1 \end{pmatrix} \begin{bmatrix} g_1 \\ g_2 \\ L' \\ 1 \end{bmatrix} \quad (11)$$

Expand the expression

$$p_1 = -\frac{f}{L}g_1 \cos \theta \cos \psi - \frac{f}{L}g_2 \cos \theta \sin \psi - \frac{fL'}{L} \sin \theta \quad (12)$$

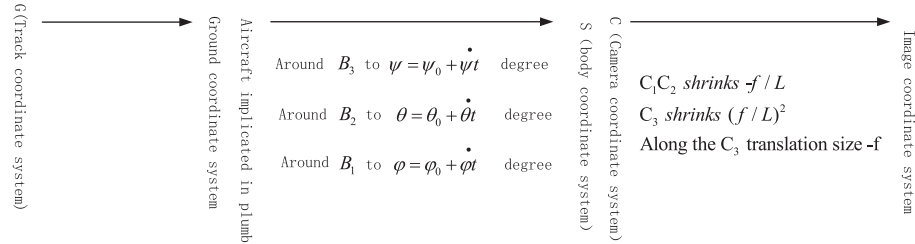


Fig. 3. Coordinate transformation process diagram.

$$\begin{aligned}
 p_2 = & \frac{f}{L} g_1 (\cos \theta \sin \psi - \sin \psi - \sin \varphi \sin \theta \cos \psi) \\
 & - \frac{f}{L} g_2 (\sin \varphi \sin \theta \sin \psi + \cos \theta \cos \psi) \\
 & + \frac{fL'}{L} \sin \varphi \sin \theta \quad (13)
 \end{aligned}
 \times \begin{pmatrix} \cos \psi & \sin \psi & 0 & 0 \\ -\sin \psi & \cos \psi & 0 & 0 \\ 0 & 0 & 1 & 0 \\ 0 & 0 & 0 & 1 \end{pmatrix} \begin{pmatrix} m_1 \\ m_2 \\ H \\ 1 \end{pmatrix} \quad (15)$$

To find the three unknowns, m_1 , m_2 and L , we expand the above matrix equations one by one to obtain the following odd linear equations.

$$\begin{aligned}
 p_3 = & \left(\frac{f}{L}\right)^2 g_1 (\cos \varphi \sin \theta \cos \psi + \sin \varphi \sin \psi) \\
 & - \left(\frac{f}{L}\right)^2 L' \cos \varphi \cos \theta \\
 & + \left(\frac{f}{L}\right)^2 g_2 (\cos \varphi \sin \theta \sin \psi - \sin \varphi \cos \psi) \quad (14)
 \end{aligned}$$

$$\begin{cases} m_1 \cos \theta \cos \psi + m_2 \cos \theta \sin \psi - H \sin \theta = 0 \\ m_1 (\sin \varphi \sin \theta \cos \psi - \cos \varphi \sin \psi) + H \sin \varphi \cos \theta \\ \quad + m_2 (\sin \varphi \sin \theta \sin \psi + \cos \varphi \cos \psi) = L \\ m_1 (\cos \varphi \sin \theta \cos \psi + \sin \varphi \sin \psi) + H \cos \varphi \cos \theta \\ \quad + m_2 (\cos \varphi \sin \theta \sin \psi - \sin \varphi \cos \psi) = 0 \end{cases} \quad (16)$$

2.4.1. Calculation of L

The speed of the ground relative to the aircraft is the ground speed $-V$. Because the image of the ground image on the image plane is an inverted image, the speed of the ground image formed on the image plane is in the direction of the image moving speed and V (the direction of flight of the aircraft), which are the same direction. When the aircraft's three attitude angles change, the feature point A (the intersection between 3 OS and the ground plane) at the center point of the image plane in Figure 3 becomes point B, generating point B in the track coordinate system. The coordinate value in G is $(0, 0, -H)$, and the coordinate value of point B in the rotated track coordinate system G' is $(0, L, 0)$. Then, the coordinates before and after the coordinate system rotate for the same point B on the ground. The value exists as shown in the following equation, the coordinate transformation relation matrix equation [38]:

$$\begin{pmatrix} 0 \\ 0 \\ L \\ 1 \end{pmatrix} = \begin{pmatrix} 1 & 0 & 0 & 0 \\ 0 & \cos \varphi & \sin \varphi & 0 \\ 0 & -\sin \varphi & \cos \varphi & 0 \\ 0 & 0 & 0 & 1 \end{pmatrix} \times \begin{pmatrix} \cos \theta & 0 & -\sin \theta & 0 \\ 0 & 1 & 0 & 0 \\ \sin \theta & 0 & \cos \theta & 0 \\ 0 & 0 & 0 & 1 \end{pmatrix}$$

$$\begin{cases} m_1 = -H \frac{\sin \theta + \cos \varphi \cos^2 \theta \sin \psi}{\sin \varphi \cos \theta} \\ m_2 = H \frac{\sin \varphi \sin \theta + \sin \theta \cos \psi + \cos \varphi \cos^2 \theta \sin \psi}{\sin \varphi \cos \theta \sin \psi} \\ L = H (c \tan \varphi \tan \theta \sin \psi + \cos \varphi \tan \varphi \cos \theta \sin^2 \psi \\ \quad - \sin \theta \tan \theta \cos \psi + \sin \varphi \cos \theta \\ \quad - \cos \varphi \sin \theta \cos \theta \sin \psi \cos \psi + \cos \varphi \sin \theta \tan \theta \\ \quad + c \tan \varphi \sin \theta \tan \theta \cos \psi \\ \quad + \cos \varphi \tan \varphi \sin \theta \cos \theta \sin \psi \cos \psi \\ \quad - \sin \varphi \tan \theta c \tan \psi - \tan \theta \cos \psi c \tan \psi \\ \quad - \cos \varphi \cos \theta \cos^2 \psi \end{cases} \quad (17)$$

2.4.2. Image Point Center Motion Calculation of the Area CCD Camera

When the initial time $t = 0$, the three-axis initial attitude angle of the aircraft is zero, $p_1 = p_2 = 0$, and the coordinates of the ground object point A corresponding to the initial image plane center point in the track coordinate system are $(0, 0, -H)$. The attitude (roll angle, pitch angle, and yaw angle) of the aircraft changes over time. The coordinate of the feature point corresponding to the center point of the image plane in the track coordinate system is the formula, and the coordinate of point A becomes (g_1, g_2, L') , in which $g_1 = -Vt$, $g_2 = 0$, with point A corresponding to the image plane coordinate system. The image plane coordinates are Ref. [39]

$$p'_1 = \frac{f}{L} Vt \cos \theta \cos \psi + f \sin \theta \quad (18)$$

$$p'_2 = \frac{f}{L} Vt (\sin \varphi \sin \theta \cos \psi - \cos \theta \sin \psi) - f \sin \varphi \sin \theta \quad (19)$$

$$p'_3 = -\left(\frac{f}{L}\right)^2 Vt (\cos \varphi \sin \theta \cos \psi + \sin \varphi \sin \psi) + \frac{f^2}{L} \cos \varphi \cos \theta \quad (20)$$

The image motions of the center point of the image plane due to the change in the aircraft flight motion and attitude angle are as follows:

The calculated forward image motion is

$$\Delta p_1 = \frac{f}{L} Vt \cos \theta \cos \psi + f \sin \theta \quad (21)$$

The horizontal image motion is

$$\Delta p_2 = \frac{f}{L} Vt (\sin \varphi \cos \psi - \cos \theta \sin \psi) - f \sin \varphi \sin \theta \quad (22)$$

2.4.3. The Image Motion Calculation of an Image Array of an Area Array Camera

When the initial time $t = 0$ is set, the three-axis initial attitude angles of the aircraft, φ , θ , ψ , are zero, any point on the planar CCD image plane $P(p_1, p_2)$, corresponds to a ground feature point $G(g_1, g_2)$, and it can be concluded that

$$g_1 = -\frac{H}{f} p_1, \quad g_2 = -\frac{H}{f} p_2 \quad (23)$$

After t , the coordinates of the feature point G in the track coordinate system are $(g_1, -Vt, g_2)$.

The corresponding image coordinates in the image plane coordinate system are

$$p'_1 = \frac{f}{L} \left(\frac{H}{f} p_1 + Vt \right) \cos \theta \cos \psi + \frac{H}{L} p_2 \cos \theta \sin \psi + \frac{fL'}{L} \sin \theta \quad (24)$$

$$p'_2 = -\frac{f}{L} \left(\frac{H}{f} p_1 + Vt \right) (\cos \theta \sin \psi - \sin \varphi \sin \theta \cos \psi) + \frac{H}{L} p_2 (\sin \varphi \sin \theta \sin \psi + \cos \theta \cos \psi) - \frac{fL'}{L} \sin \varphi \sin \theta \quad (25)$$

The forward image motion is

$$\Delta p_1 = \frac{f}{L} \left(\frac{H}{f} p_1 + Vt \right) \cos \theta \cos \psi + \frac{H}{L} p_2 \cos \theta \sin \psi + \frac{fL'}{L} \sin \theta - p_1 \quad (26)$$

The horizontal image motion is

$$\Delta p_2 = -\frac{f}{L} \left(\frac{H}{f} p_1 + Vt \right) (\cos \theta \sin \psi - \sin \varphi \sin \theta \cos \psi) + \frac{H}{L} p_2 (\sin \varphi \sin \theta \sin \psi) - \frac{fL'}{L} \sin \varphi \sin \theta - p_2 \quad (27)$$

2.5. Image Motion Diagram in Different Situations

As shown in Figure 4, in the case of a vertical photograph of the ground, under the conditions of different aircraft flight speeds, different attitude angles, etc., the image motion vector at each point on the CCD area array calculated by the azimuth element method is obtained. Among them, (a) and (b) show the image motion caused by the different flight speeds of the aircraft when the attitude angle of the aircraft is zero. From the comparison of the two diagrams, it can be seen that the CCD image plane increases with increased aircraft flight speed. The larger is the image motion caused, the larger is the image motion at each point on the image surface of the CCD. In addition, the direction is the same, with all motions in the opposite direction of the flight direction of the aircraft, and (c) and (d) only change the roll angle of the aircraft. When the pitch angle, the yaw angle and the flight speed of the aircraft are all zero, the image motion vector diagram can be seen from the comparison of the two diagrams. The image motion caused by the aircraft's orientation increases as the aircraft roll angle increases. In addition, the image motions at the points on the CCD image surface are the same, and the directions are the same, with (c) and (d) showing that only the roll angle of the aircraft is changed, and the pitch angle, the yaw angle, and the aircraft flight speed are all zero. The image motion vector diagram shows that the greater is the roll angle of the aircraft, the greater is the image motion caused by the aircraft's spread with the same magnitude and direction of the image motions at each point on the CCD image plane. In this case, (f) and (g) show that only the aircraft's pitch angle is changed, and the roll angle, yaw angle, and flight of the aircraft are all zero. When the degrees are zero, the image motion caused by the vector diagram can be seen from the comparison of the two graphs. The larger is the pitch angle of the aircraft, the greater are the image motion caused by the flight direction of the aircraft and the image motion of each point on the CCD image plane. In the same size and direction, by comparing (g), (h), (i) and (j), it can be seen that when the aircraft's pitch angle is properly changed in accordance with the specified positive direction, the flight motion due to the aircraft can be reduced [40].

Concerning the amount of image motion caused on the CCD image plane, (k) and (l) show the image motion caused by changing only the yaw angle of the airplane, and the roll angle, pitch angle, and aircraft flying speed

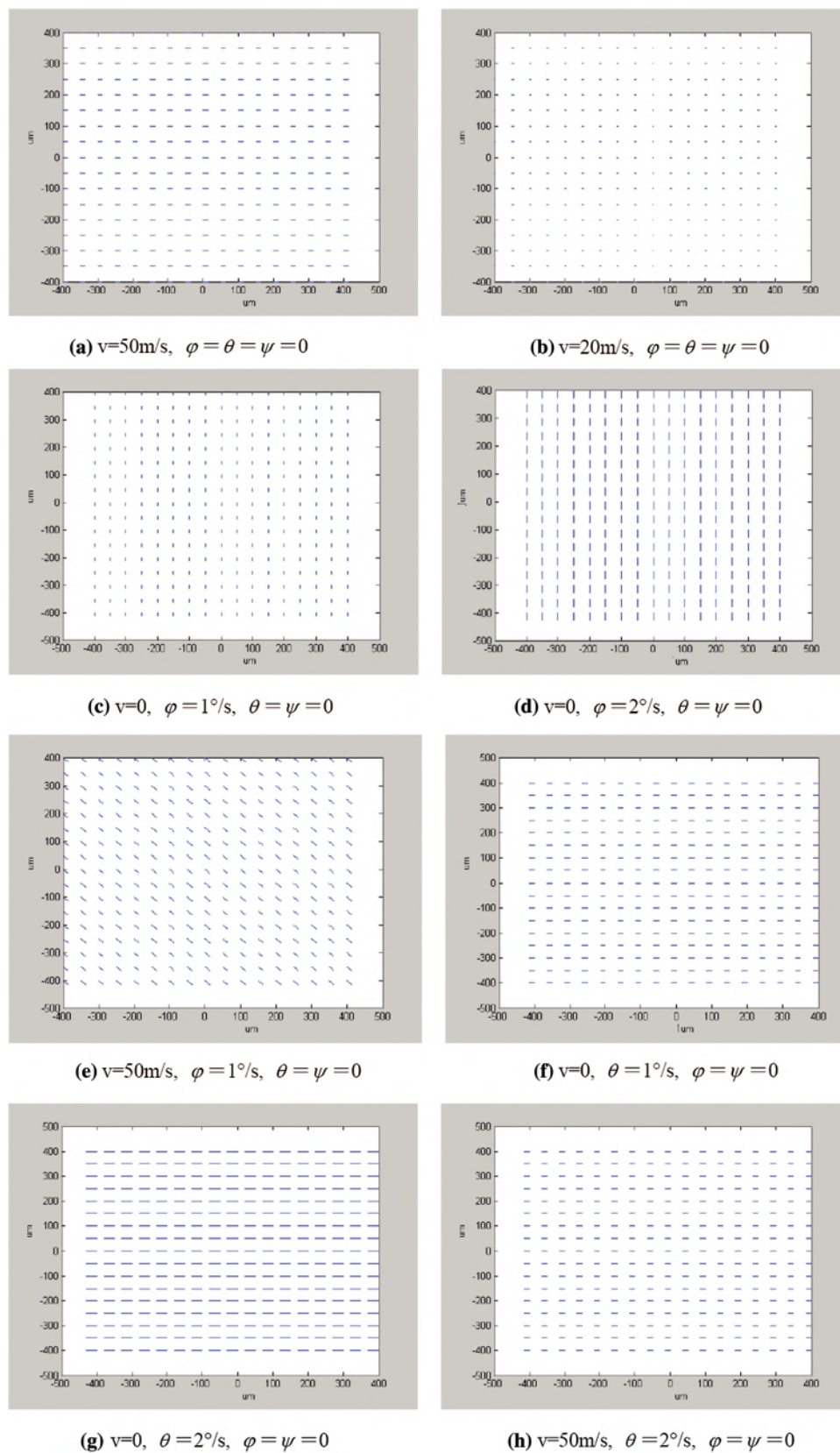


Fig. 4. Continued.

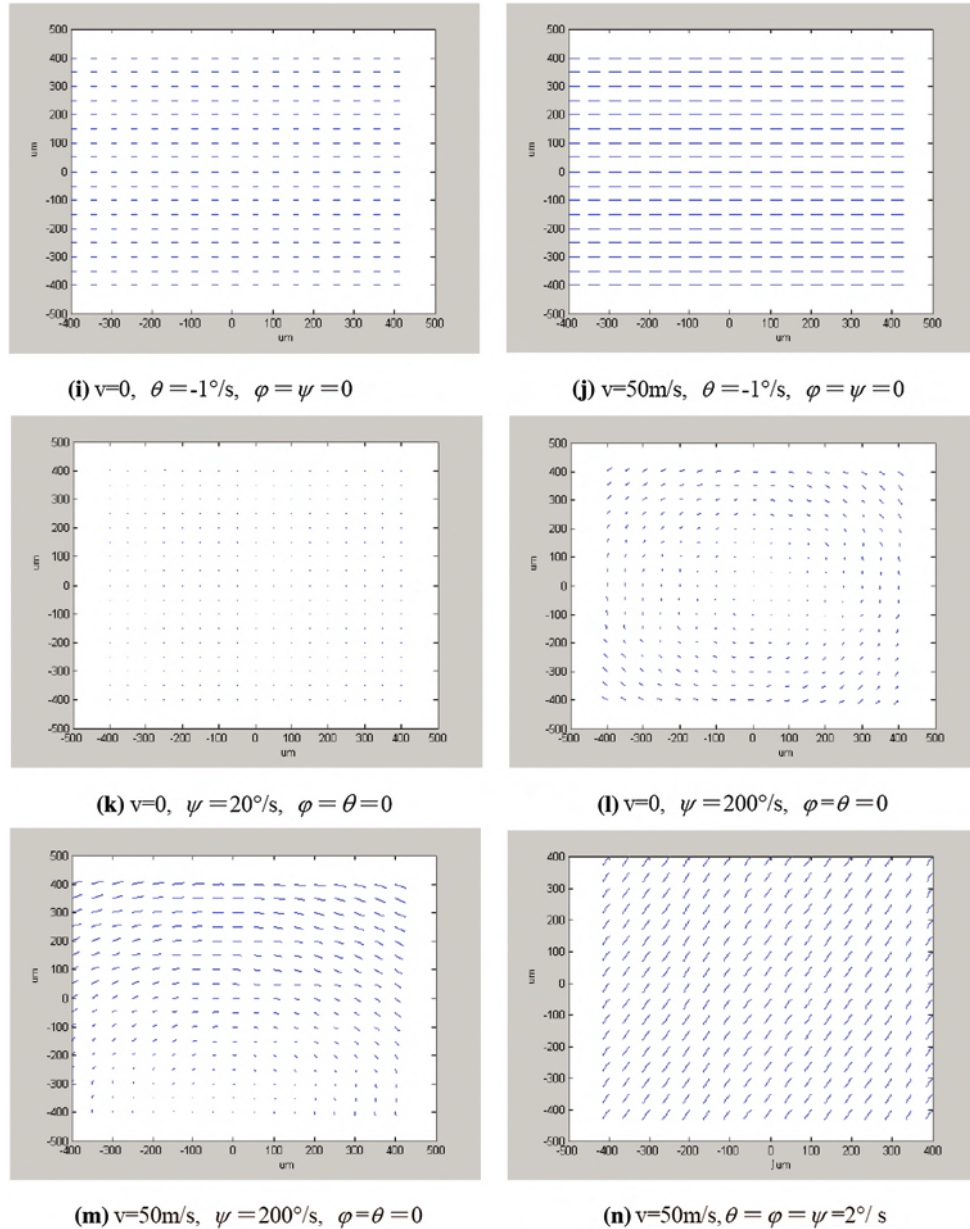


Fig. 4. CCD array image shift vector of different conditions.

are all zero. From the comparison of the two diagrams, it can be seen that the image motion increases with increasing of the aircraft yaw angle, and the image motions at each point on the CCD image surface are different and in different directions. The aircraft can be seen from the diagram. The image motion caused by yaw is much smaller than that caused by other attitude changes [41].

3. IMAGE MOTION COMPENSATION TECHNOLOGY FOR THE CCD AREA ARRAY

Considering the production cost, volume limit, domestic process status, and system index requirements of the CCD area array mapping camera system, after analyzing and

comparing the application conditions of the above methods, a three-axis stabilization platform is added between the focal plane and the aircraft. The method is used to compensate for the image movement caused by aircraft movement and attitude changes and to overcome the influence of vibration and in-flight drag torque on image quality. A vibration absorber is added between the aircraft and the triaxial stabilization platform to isolate the high-frequency vibration. At the same time, the sampled rotary pitch axis correction method compensates for the compensation caused by aircraft flight motion.

3.1. Front Image Motion Compensation

In the process of photographing using the area CCD mapping camera, the pitch axis swings at a constant angular

velocity A (refer to Chapter 3 for the calculation of ω_c). In the speed control mode, the motion period is the same as the photographing period. The working process is as follows. At the end of one shot, the pitch axis moves quickly along the flight direction to a certain fixed position (according to the ratio of the speed-to-height ratio, the size of the surface array digital camera target surface, etc.), and then it is photographed at an angular velocity ω_c and in the reverse direction of the flight at a constant speed. The above process is repeated to complete the image motion compensation process [42].

The calculation time interval T of the CCD area array camera is calculated as follows:

$$T = (1 - \eta)H/V \times A/f \tag{28}$$

The heading overlap rate in the formula is $\eta = 60\%$.

A —CCD area size, $4096 \times 0.009 = 36.86$ mm; H —3000 m to 5000 m; and V —Reaches up to 180 km/h.

The central control system of the CCD area array mapping camera calculates the shooting interval based on V and H and continuously shoots according to a predetermined program. As shown in Table I.

3.2. Image Motion Compensation Due to Pitch, Yaw and Roll

The CCD area array camera compensates for the image motion caused by changes in the aircraft attitude. By adopting three axes (pitch, azimuth, and roll axes) of a three-axis stabilized platform, the angular rate is equal to the aircraft attitude change rate and in the opposite direction.

When the attitude of the aircraft changes, to compensate for the induced image motion, the CCD area array camera compensates for the image motion caused by the aircraft's change in attitude by adding a three-axis gyro-stabilizing platform between the aircraft body and the camera's optical system and focal plane. The specific implementation process is that when the control system receives information on a change in the aircraft's three attitudes. The servo controller controls the rotation of the three axes of the three-axis gyro stabilization platform, and the direction of rotation of the three axes is opposite to that of the aircraft attitude to achieve the compensation effect. Therefore, the residual image motion caused by compensating for aircraft attitude changes mainly depends on the accuracy of the servo control system in controlling the three-axis gyro stabilization platform of the CCD area array camera. When

Table I. Photography interval T value (units: s).

V	H	
	3000 m	5000 m
150 km/h	12.1	20.2
180 km/h	10.2	15.7

yaw, pitch and roll angles are generated when the attitude of the aircraft changes, the angle between the direction of the aircraft's speed and the direction of the speed when the initial aircraft does not change posture is the yaw angle. The direction of the camera motion compensation speed changes with the attitude change, and the camera shifts. The magnitude of the compensation speed is determined by the components of the aircraft speed in the three axis directions after the rotation of the coordinate system [43–44].

Let these three components be V_x, V_y, V_z .

$$\begin{bmatrix} V_x \\ V_y \\ V_z \end{bmatrix} = \begin{pmatrix} 1 & 0 & 0 \\ 0 & \cos \alpha & \sin \alpha \\ 0 & -\sin \alpha & \cos \alpha \end{pmatrix} \begin{pmatrix} \cos \theta & 0 & -\sin \theta \\ 0 & 1 & 0 \\ \sin \theta & 0 & \cos \theta \end{pmatrix} \times \begin{pmatrix} \cos \psi & \sin \psi & 0 \\ -\sin \psi & \cos \psi & 0 \\ 0 & 0 & 1 \end{pmatrix} \begin{bmatrix} V \cos \psi \\ V \sin \psi \\ 0 \end{bmatrix} \tag{29}$$

$$\begin{cases} V_x = V(\cos \theta \cos^2 \psi + \cos \theta \sin^2 \psi) \\ V_y = V(\sin \alpha \sin \theta \cos^2 \psi - \cos \alpha \sin \psi \cos \psi + \sin \alpha \sin \theta \sin^2 \psi + \cos \alpha \cos \psi \sin \psi) \\ V_z = V(\cos \alpha \sin \theta \cos^2 \psi + \sin \alpha \sin \psi \cos \psi + \cos \alpha \sin \theta \sin^2 \psi - \sin \alpha \cos \psi \sin \psi) \end{cases} \tag{30}$$

3.3. Application of the Orthogonal Projection Decomposition Method in Image Motion Calculation

As shown in Figure 5, at the instant of exposure of the vertically placed aerial camera, due to the flying motion of the aircraft, the ground object A moves relative to the aircraft to position A' , and the point of motion moves to a' , causing the influence to move if it is exposed to the camera. At the same time, by properly moving the CCD, the image point a can be relatively stationary.

The angular velocity of the pitch axis is calculated as follows: the image point formed by the center projection

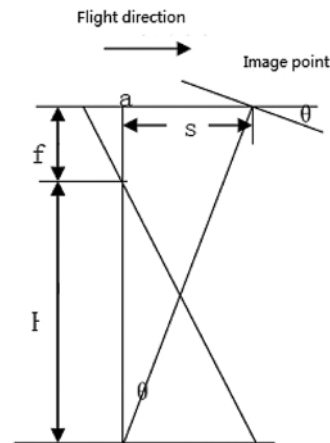


Fig. 5. Chart of compensation speed calculation.

Table II. Image shift values due to rounding errors.

Height	Exposure time			
	1/1000 s	1/500 s	1/250 s	1/100 s
3000	0.6101	0.6102	0.6204	0.6109
5000	0.19	0.19	0.1901	0.1902

on the image plane at the start of exposure is a , and the image point moves to a' after exposure at time t . The image motion amount at point a after t is

$$s = v_{imc} t \quad (31)$$

When the image motion s is compensated using the method of rotation of the pitch axis, the rotational angular speed of the pitch axis is

$$\theta = \arctg(s/(f + H)) \quad (32)$$

θ —Rotation angle of the pitch axis; s —Flight distance of the aircraft during the exposure of the camera, $s = vt$; t —Exposure time; V —Speed of the aircraft; f —Camera focal length; and H —Aircraft altitude.

Since $f, s \ll H$, $\omega_c = V/H$, Eq. (32) can be simplified to $\omega_c = V/H$.

The image motion caused by calculating the rounding error is shown in Table II, where the exposure time is 1/1000 s, 1/500 s, 1/250 s, and 1/100 s, $f = 90$ mm, and V is 50 m/s (maximum speed). H is 3000 m (the minimum height) and 5000 m [45].

As seen from the Table II, the amount of paraxial image motion caused by the calculation of the rounding error does not exceed 1/3. The elemental ($3 \mu\text{m}$) effect on imaging quality can be ignored. The orthogonal projection analysis method is characterized by considering the main factors, ignoring the secondary factors, considering the independent action components of each factor, and ignoring the coupling action components. This method has a simple expression and employs easy calculations. This method is easy to use for engineering, but there is a certain image motion error after compensation, and it is difficult to calculate the amount of image motion with this method for complex optical systems [46].

4. THE ANALYSIS AND CALCULATION OF IMAGE MOTION RESIDUAL ERRORS

Full compensation is always difficult to achieve through image motion compensation. Starting from system development, it is necessary to propose a reasonable accuracy requirement, that is, a way to meet the requirements of image motion compensation. Under the conditions developed by the digital aerial camera, the minimum requirement on the median error of the remaining image motions after image motion compensation is that it should be no

more than 1/3 of a pixel. For example, if the pixel size is $9 \mu\text{m}$, the error from the remaining image motion values after image motion compensation should be less than $3 \mu\text{m}$. The residuals compensated by various image motion compensation methods are not the same. This section analyzes and calculates the image motion residuals of the system based on the pitch rotation compensation method used by the surveying and mapping system.

4.1. Accuracy Analysis of the Pitch Rotation Compensation Method

The pitch compensation method is an approximate image motion compensation method because this method does not take into account the deviation of the y -direction image coordinates caused by the pitch rotation, which in turn causes blurring in the y -direction image.

Let α be the pitch rotation compensation angle.

$$\alpha = \arctg \frac{Vt}{H} \quad (33)$$

As seen from Formula (33), the accuracy of this compensation method depends on the accuracies of the speed, altitude, and exposure time of the camera shutter provided by the system, and the error model of the pitch rotation compensation method can be obtained.

$$d\alpha = \frac{1}{1 + (Vt/H)^2} \left(\frac{tdV + Vdt}{H} - \frac{VtdH}{H^2} \right) \quad (34)$$

Since $Vt \ll H$, rounding off the second item,

$$d\alpha = \frac{tdV + Vdt}{H} - \frac{VtdH}{H^2} \quad (35)$$

From the error model, the precision estimation model of the method can be derived.

$$m_\alpha = \pm \sqrt{V^2 m_t^2 + t^2 m_v^2 + \frac{T^2 V^2}{H^2} m_h^2} \quad (36)$$

In the formula, m_α is the middle error of the image motion compensation; m_t is the middle error of the camera shutter exposure time; m_v is the error of the aircraft speed; and m_h is the aircraft mid-range error [47].

Since the system must be equipped with a precision pilot GPS subsystem, the altitude error can be set to 10 m. Due to the relatively high accuracy of the GPS system, m_v can be set to 1 m/s, and the accuracy of the camera shutter exposure time can generally reach 1/10 of the exposure time. Figure 6 shows the mid-error curve of the pitch compensation for image motion compensation due to errors in aircraft speed, mid-course altitude errors, and exposure time errors, wherein the focal lengths are both 90 mm, and Figure 6(a) shows the same data at an altitude of 3000 m with the image motion versus exposure time from 10 m/s to 50 m/s [48].

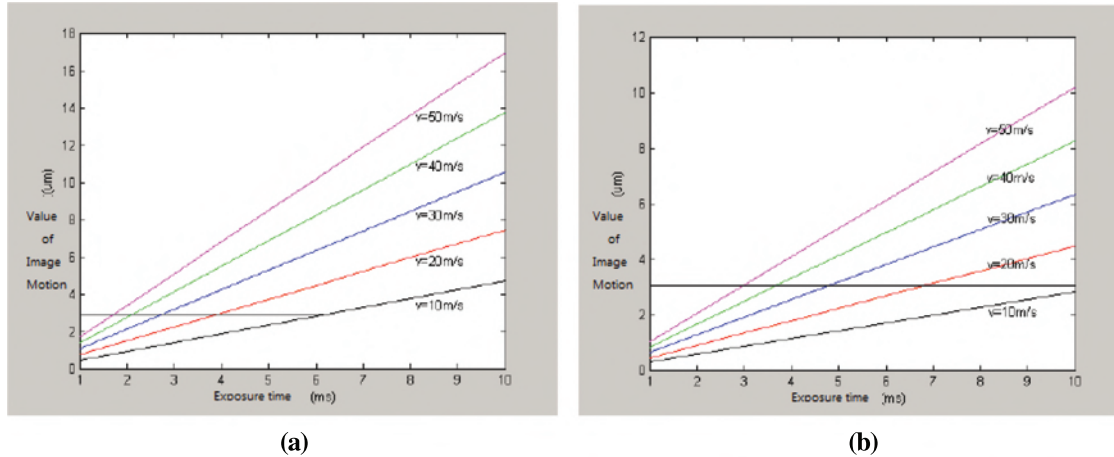


Fig. 6. Pitch compensation image motion due to accuracy. (a) Shows the same data at an altitude of 3000 m with the image motion versus exposure time from 10 m/s to 50 m/s. (b) Shows the same data at an altitude of 5000 m with the image motion versus exposure time from 10 m/s to 50 m/s.

As seen from Figure 6 above, the slower the flight of the aircraft, the higher is the altitude, and the shorter the exposure time, the smaller are the errors in image motion compensation. When the altitude is 5000 m and the speed is 10 m/s, the middle error of the image motion compensation caused by each medium error in each exposure time of the system does not exceed $3 \mu\text{m}$. When the speed is 50 m/s, only the exposure time is less than 3 ms. To obtain high compensation accuracy, the mid-error of the image motion compensation due to each medium error does not exceed $3 \mu\text{m}$, and other longer exposures exceed $3 \mu\text{m}$ and cannot meet the requirements of image motion compensation. When the altitude is 3000 m, the speed is 50 m/s and the exposure time is less than 1.6 ms, the medium shift error due to each medium error does not exceed $3 \mu\text{m}$, and other longer exposures exceed $3 \mu\text{m}$, a condition that cannot be satisfied. Similar to shift compensation requirements, to obtain high compensation accuracy, a high-precision pilot GPS subsystem must be configured [49].

4.2. Image Motion Residual Errors

To calculate the residuals compensated by the image motion compensation system, the discussion of image motion is decomposed into discussions of the image motion caused by the aircraft's flight motion and the image motion due to the change in the aircraft's attitude. Based on this discussion, the aircraft movement due to compensation is discussed separately. The residuals and the residuals that compensate for the change in attitude of the aircraft will be added in the same direction to obtain the total residual amount. The aircraft's flight speed is assumed to be zero when considering the compensation residual due to aircraft attitude change, and the attitude angle of the aircraft is assumed to be zero when analyzing and calculating the aircraft movement speed caused by the aircraft's flight speed compensation error.

4.2.1. Image Motion Compensation Residuals of Aircraft Attitude Changes

When the attitude of the aircraft changes, to compensate for the image motion caused by that change, the CCD area array camera adopts a method that adds a three-axis gyro-stabilizing platform between the aircraft body, the camera optical system and the focal plane to compensate for the image motion caused by the aircraft attitude change. The specific implementation process is that when the control system receives the three pieces of attitude change information for the aircraft, the servo controller controls the three axes of the three-axis gyro stabilization platform to rotate, and the direction of rotation is opposite to that of the aircraft attitude, thereby achieving a compensating effect. Therefore, the image motion residual caused by compensating for aircraft attitude changes mainly depends on the accuracy of the servo control system in controlling the three-axis gyro stabilization platform of the CCD area array camera. From Chapter 5, we know that the control accuracy of the triaxial stability platform is $0.1^\circ/\text{s}$, that is, the compensated equivalent aircraft attitude angle rate is $0.1^\circ/\text{s}$, the exposure times are $1/1000 \text{ s}$, $1/500 \text{ s}$, $1/250 \text{ s}$, and $1/100 \text{ s}$, $f = 90 \text{ mm}$, V is 50 m/s (maximum speed), H is 3000 m (minimum height), and the difference in the image motion due to aircraft attitude change is shown in Figure 7 [50–53].

As seen from Figure 7, the residual image motion compensation error of the CCD area array camera is less than $1/3$ pixel, which meets the requirements of the imaging system.

The attitude angle of the aircraft is zero when using the coordinate transformation method to calculate the image motion (image advancement) caused by aircraft flight compensation residuals, i.e., $\varphi = \theta = \psi = 0$. Because the CCD area array camera adopts the pitch axis of the rotating triaxial stable platform to compensate for image advancement, when calculating the image motion compensation residual, it can be equivalent to the aircraft's

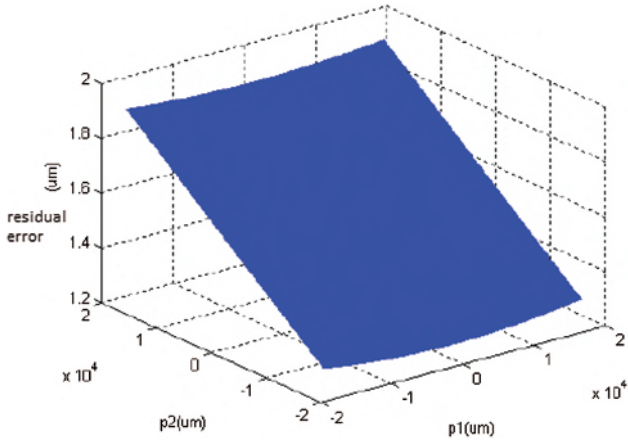


Fig. 7. Attitude compensation residual map.

flying speed V , and the aircraft's pitch angle is $t Vt$. The computation of image motions when $\theta = \omega_{imc}t = -Vt/H$ is as follows.

$$\begin{pmatrix} 0 \\ 0 \\ L \end{pmatrix} = \begin{pmatrix} \cos \theta & 0 & -\sin \theta \\ 0 & 1 & 0 \\ \sin \theta & 0 & \cos \theta \end{pmatrix} \begin{pmatrix} m_1 \\ m_2 \\ H \end{pmatrix} \quad (37)$$

This equation is solved as follows:

$$\begin{cases} m_1 = H \tan \theta \\ m_2 = 0 \\ L = H / \cos \theta \end{cases} \quad (38)$$

The forward image motion is

$$\begin{aligned} \Delta p_1 &= p'_1 - p_1 \\ &= \frac{fVt}{H} \cos^2 \theta + \frac{fL'}{H} \sin \theta \cos \theta - p_1 \sin^2 \theta \end{aligned} \quad (39)$$

The horizontal image motion is

$$\Delta p_2 = p'_2 - p_2 = 0 \quad (40)$$

The total image motion residual is

$$\Delta p = \sqrt{\Delta p_1^2 + \Delta p_2^2} = |\Delta p_1| \quad (41)$$

As shown in Figure 8, the image motion residual image of the CCD area array is calculated by using the coordinate transformation method. From Figure 8, it can be seen that the image motion compensation residual at any point

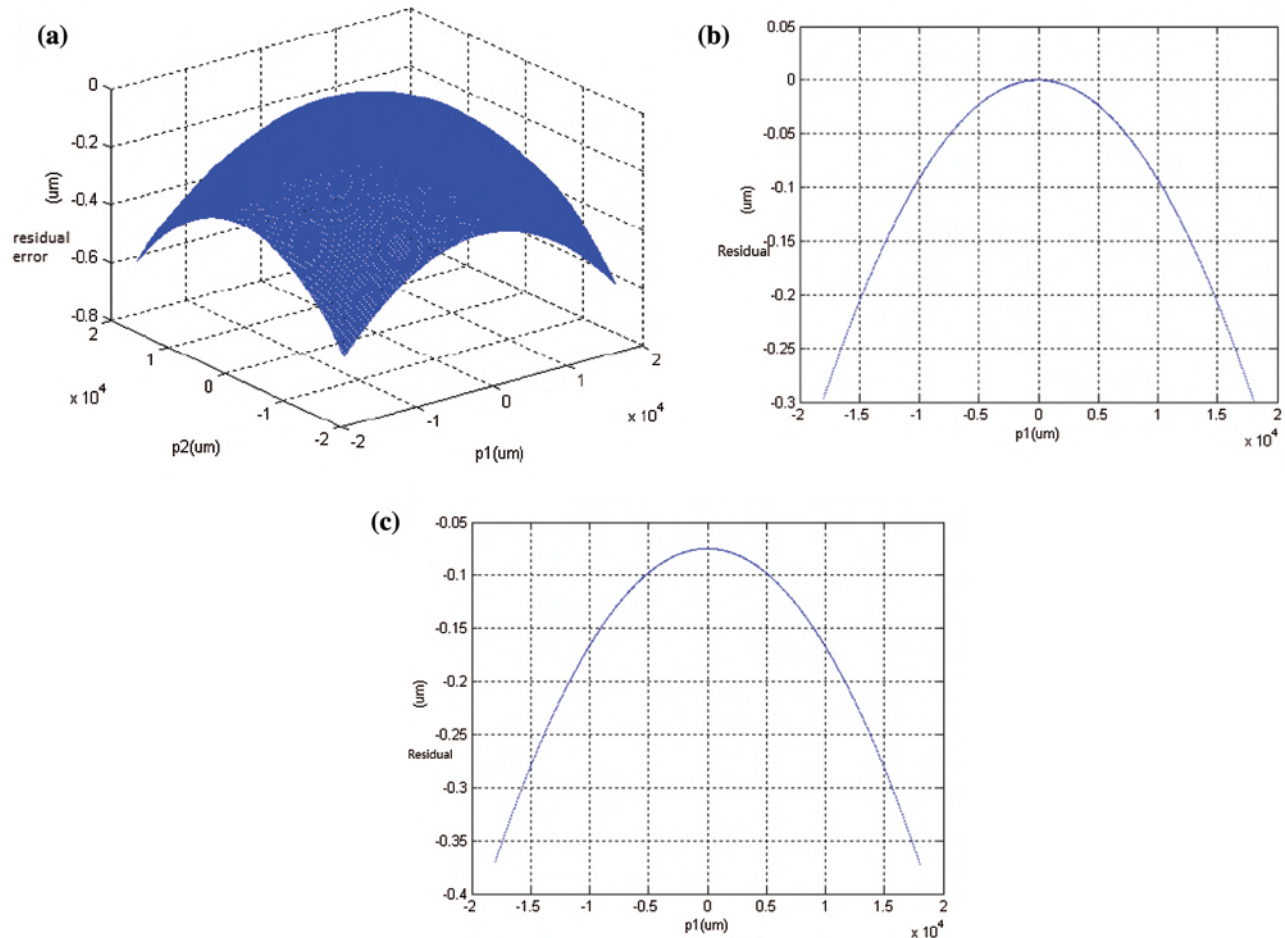


Fig. 8. Image motion compensation residual map.

on the image plane does not exceed 1/3 of a pixel. The minimum value is at the center of the image plane.

Figure 8(a) shows the image motion residuals when the aircraft's flight height is 3000 meters. The residual map when $p_2 = 0$ is shown in (b), and that for $p_2 = 900 \mu\text{m}$ is shown in (c).

Comparing (a), (b), and (c), it can be seen that the image motion compensation residuals at each point on the same column are distributed symmetrically around the center point, and the image motion compensation residuals are larger at the image point farther from the center point. Similarly, the image motion compensation residuals at each point on the same line are symmetrically distributed around the center point, and the image motion compensation residual increases with increasing distance from the center point.

Although the rotary pitch axis compensation method can meet the requirements of the CCD area array mapping camera, if the camera's focal plane is enlarged, the use of this method to compensate for camera image advancement is limited, as shown in Figure 8. If one does not consider the size of the camera focal plane, under the conditions of the camera's speed, height, etc., formulas (6–7) can be calculated when the image plane size is less than $9\text{ K} \times 9\text{ K}$, using the focal plane rotation method to compensate the image. The displacement residuals are all less than $3 \mu\text{m}$, and when the image plane size is larger than $9\text{ K} \times 9\text{ K}$, the angle θ between the ground point and the image plane center satisfies the condition $|\theta| > 35^\circ$, and the imaging system requirements cannot be met, as shown in Figure 9. Therefore, the focal plane is used. The rotation compensation method has a certain angle limit for the image advancement compensation. When the pitch angle of the pitch axis does not exceed 12° , the imaging requirement can be satisfied by using the rotary pitch axis to compensate for the image advancement [54–56].

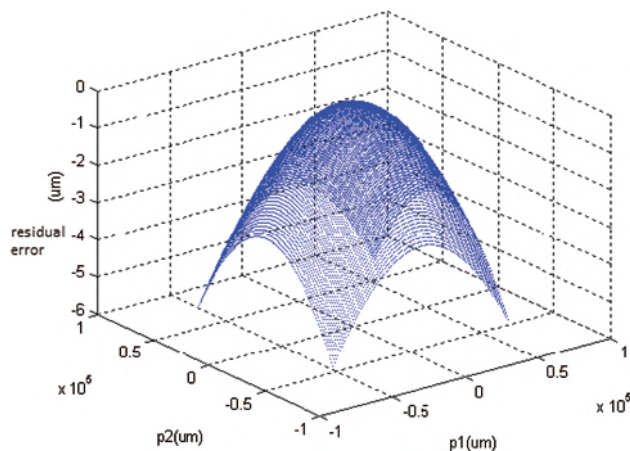


Fig. 9. Residual map after an extended image.

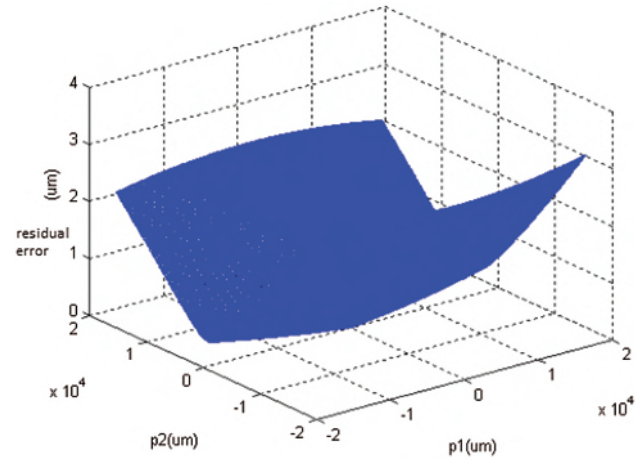


Fig. 10. Overall residual map.

4.2.2. Total Image Motion

The total residual image compensation error of the CCD area array camera is equal to the sum of the image advancement compensation residual and the attitude compensation residual. The image total residual distribution map is shown in Figure 10. From Figure 10, it can be seen that the image motion compensation residual is the smallest at the center of the image plane, and the residual is large at the edge of the image plane. Overall, however, the use of a triaxial stabilization platform to compensate for image motions caused by aircraft flight and attitude changes is feasible and meets the requirements of the imaging system. The total residual image motion of any pixel on the image plane is less than 1/3 of a pixel.

5. CONCLUSIONS

In this paper, the working principle of a CCD array surveying camera and a method for compensating for image shifts are studied and analyzed. A three-axis stabilized platform is added between the camera and the plane, the three axes of the rotating platform are compensated by the three axes of the rotating platform, and the forward flight motion of the plane is made using the rotating pitch axis compensation. The image shift calculation method is discussed, and coordinate transformation is applied to the image shift calculation of the CCD surface array camera. The principle is to identify the image shift by the matrix relation between the coordinates of the image points on the image surface before and after the camera attitude transformation. In addition, the coordinate transformation method for mapping the CCD array is introduced in detail. The calculation of the angular velocity of the camera motion compensation and the image quality and image motion residuals of the CCD camera after image motion compensation are analyzed. The coordinate transformation method is used to calculate that the method of compensating for the image forward motion by rotating the pitch axis and can satisfy the imaging requirement when the pitch angle

of the pitch axis does not exceed 12 degrees. The residual error of attitude image motion compensation is less than $3 \mu\text{m}$, which meets the imaging requirement. It is proven that the image motion compensation method and control algorithm designed in this paper meet the system requirements.

Conflicts of Interest

The authors declare no conflict of interest.

Acknowledgments: This work was supported by the National Natural Science Foundation of China (Grant No. 62175233).

References and Notes

- Janschek, K. and Tchemykh, V., **2001**. Optical Correlator for Image Motion Compensation in the Focal Plane of a Satellite Camera. *Proceedings of the 15th IFAC Symposium on Automatic Control in Aerospace*, September 2–7; Bologna, Italy. pp.378–382.
- Lareau, A.G., Beran, S.R., Lund, J.A. and Pfister, W.R., **1992**. Electro-Optical Imaging Array with Motion Compensation. U.S. Patent 5,155,597.
- Hussain, R., Noyan, M.A., Woyessa, G., Retamal Marín, R.R., Martinez, P.A., Mahdi, F.M., Finazzi, V., Hazlehurst, T.A., Hunter, T.N., Coll, T., Stintz, M., Muller, F., Chalkias, G. and Pruneri, V., **2020**. An ultra-compact particle size analyser using a CMOS image sensor and machine learning. *Light Sci. Appl.*, 9(21), DOI: 10.1038/s41377-020-0255-6.
- Olson, G.G., **2002**. Image Motion Compensation with Frame Transfer CCDs. *Proc. SPIE*, Vol. 4567, pp.153–160.
- Bosiers, J.T., Kleimann, A.C., van Kuijk, H.C., Le Cam, L., Peek, H.L., Maas, J.P. and Theuwissen, A.J., **2002**. Frame transfer CCDs for digital still cameras: Concept, design, and evaluation. *IEEE Trans. Electron. Devices*, 49, pp.377–386.
- Li, D.-Y., Xia, Q., Yu, T.-T., Zhu, J.-T. and Zhu, D., **2021**. Transmissive-detected laser speckle contrast imaging for blood flow monitoring in thick tissue: From monte carlo simulation to experimental demonstration. *Light Sci. Appl.*, 10(241), DOI: 10.1038/s41377-021-00682-8.
- Markelov, S.V., Murzin, V.A., Borisenko, A.N., Ivaschenko, N.G., Afanasieva, I.V. and Ardilanov, V.I., **2000**. A high-sensitivity CCD camera system for observations of early universe objects. *Astronom. Astrophys. Trans.*, 19, pp.579–583.
- Gach, J.L., Darson, D., Guillaume, C., Goillandeau, M., Cavadore, C., Balard, P., Boissin, O. and Boulesteix, J., **2003**. A new digital CCD readout technique for ultra-low-noise CCDs. *Astronom. Soc. Pac.*, 115, pp.1068–1071.
- Gach, J.L., Darson, D., Guillaume, C., Goillandeau, M., Boissin, O., Boulesteix, J. and Cavadore, C., **2004**. Zero Noise CCD: A New Readout Technique. *Science Detectors for Astronomy*. Springer, Dordrecht, The Netherlands. pp.603–610.
- Papaioannou, M., Plum, E., Rogers, E.T. and Zheludev, N.I., **2018**. All-optical dynamic focusing of light via coherent absorption in a plasmonic metasurface. *Light Sci. Appl.*, 7, p.17157, DOI: 10.1038/lsa.2017.157.
- Wu, S., Cheng-Shan, H., Heng-yi, L., Xu-cheng, X. and Chang-Hong, H., **2019**. Dynamic range extending method for push-broom multispectral remote sensing cameras. *Chinese Optics*, 12(4), pp.905–912.
- Hu, H., Lin, X., Wong, L.J., Yang, Q., Liu, D., Zhang, B., Luo, Y., **2021**. Surface Dyakonov-Cherenkov radiation. *eLight*, 2(2022), DOI: 10.1186/s43593-021-00009-5.
- Smith, S.L., Mooney, J., Tantaló, T.A. and Fiete, R.D., **1999**. Understanding image quality losses due to smear in high-resolution remote sensing imaging systems. *Optical Engineering*, 38(5), pp.821–826.
- Miller, B.M. and Rubinovich, E.Y., **2007**. Image motion compensation at charge-coupled device photographing in delay-integration mode. *Automation and Remote Control*, 68(3), pp.564–571.
- James, C. and Bremer, **1999**. Scanning technique for advanced geosynchronous studies imager: Conical scanning to compensate for image rotation. *SPIE*, 9, pp.35–46.
- Zhang, B.Y., Kong, D.Z., Liu, J.G., Wu, X.X. and Dong, D.Y., **2020**. Compensation of star image motion for a CMOS image sensor with a rolling shutter. *Chinese Optics*, 13(6), pp.1276–1284.
- Vallapureddy, S.R., Banyal, R.K., Rengaswamy, S., Kamath, P.U., and Selvaraj, A., **2020**. Development of image motion compensation system for 1.3 m telescope at vainu bappu observatory. *Research in Astronomy and Astrophysics*, 20(1), p.12.
- Ustun, D., **2020**. An enhanced adaptive butterfly optimization algorithm rigorously verified on engineering problems and implemented to ISAR image motion compensation. *Engineering Computations*, 37(9), pp.3543–3566.
- Ramachandran, M., Agarwal, M.K. and Daniel, D.A., **2020**. Efficient onboard image motion compensation for orbital inclination and eccentricity of geostationary weather satellites. *Proceedings of the Institution of Mechanical Engineers Part G Journal of Aerospace Engineering*, DOI: 10.1177/0954410019900706.
- Holst, G.C., **1998**. *CCD Arrays, Cameras, and Displays*. 2nd edition, USA, JCD Publishing, Willmann-Bell.
- Shuqing, Z., Yuan, Z., Chenghao, Z. and Zhile, W., **2014**. Image motion model of azimuthally photography for satellite borne TDICCD camera. *Infrared and Laser Engineering*, 43(6), pp.1823–1829.
- Shuqing, Z. and Tao, L., **2014**. Analysis on different rates image motion of space camera with a scanning mirror. *Acta Optica Sinica*, 34(2), p.0228006(in chinese).
- Yong-Sen, X., Ya-Lin, D., Hai-Ying, T., et al., **2007**. Calculation and compensation for image motion of aerial remote sensor in oblique situation. *Optics and Precision Engineering*, 15(11), pp.1779–1783.
- Lei, Z., Ya-Lin, D., Hong-Wen, Z. and Hu, L., **2009**. Methods and theories analysis of image motion compensation based on LOROP cameras. *LASER & INFRARED*, 39(4), pp.423–426.
- Tang, R., Fritsch, D., Cramer, M. and Schneider, W., **2012**. A flexible mathematical method for camera calibration in digital aerial photogrammetry. *Photogrammetric Engineering and Remote Sensing*, 78(10), pp.1069–1077.
- Wang, L., Liu, X. and Wang, C., **2019**. Modeling and design of fast steering mirror in image motion compensation for backscanning step and stare imaging systems. *Optical Engineering*, 58(10), p.1.
- Chen, W., Lei, Y. and Yang, H., **2019**. Research on the Fast Image Motion Compensation Technology of Aerial Digital Camera. *The 2nd International Conference*, pp.71–74, DOI: 10.1145/3341016.3341641.
- Xiu, J., Huang, P., Li, J., Zhang, H. and Li, Y., **2020**. Line of sight and image motion compensation for step and stare imaging system. *Applied Sciences*, 10(20), p.7119.
- Chun-Feng, Y., Zhi-Chao, C., Ping, J., Nai-Xiang, W. and Han, H., **2020**. Analysis of the effect of lens shutter on image motion in aerial camera. *Chinese Optics*, 13(3), pp.616–626.
- Tian, D., Wang, Y., Wang, Z., Wang, F. and Gao, H., **2019**. Long integral time continuous panorama scanning imaging

- based on bilateral control with image motion compensation. *Remote Sensing*, 11, p.1924.
31. Wang, D.J., Zhang, T. and Kuang, H.P., 2011. Clocking smearing analysis and reduction for multi phase TDI CCD in remote sensing system. *Optics Express*, 19(6), pp.4868–4880.
 32. Li-Zhi, X., Yi, L. and Zhi-Yuan, G., 2019. Image motion calculation and error distribution for aerial whisk-broom imaging. *Optics and Precision Engineering*, 27(10), pp.2071–2079.
 33. Peng-Luo, L., Yong-Chang, L., Long-Xu, J., Guo-Ning, L., Yi-Nan, W. and Wen-Hua, W., 2016. Image motion velocity field model of space camera with large field and analysis on three-axis attitude stability of satellite. *Optics and Precision Engineering*, 24(9), pp.2173–2182.
 34. Shao-Xin, W., Ke-Qi, Q., Yu-Kun, W., Zhi, W. and Li-Heng, C., 2019. Study on loss of performance in inertial sensors due to electrode asymmetry. *Chinese Optics*, 12(3), pp.455–462.
 35. Jian-Rong, W., Ren-xiang, W. and Xin, H., 2019. On-orbit calibration of camera parameters based on line-matrix charge-coupled device imagery. *Optics and Precision Engineering*, 27(4), pp.984–989.
 36. Zheng-Xi, W., Bao, Z., Xian-Tao, L.I. and Shi-tao, Z., 2020. Application of fast steering mirror in image motion compensation. *Chinese Optics*, 13(1), pp.95–105.
 37. Chun-Feng, Y., Zhi-Chao, C., Ping, J., Nai-Xiang, W. and Han, H., Analysis of the effect of lens shutter on image motion in aerial camera. *Chinese Optics*, 13(3), pp.616–626.
 38. Cheng-Hao, L., Xu, H., Qi, J., Xiao-Hui, Z. and Ning, L., 2020. Design of high spatial and temporal resolution dynamic star simulator. *Editorial Office of Optics and Precision Engineering*, 28(3), pp.515–525.
 39. Li-Zhi, X., Chang-Xiang, Y., Yi, L. and Zhi-Yuan, G., 2019. Image motion calculation and error distribution for aerial whisk-broom imaging. *Optics and Precision Engineering*, 27(10), pp.2071–2079.
 40. Peng, L., Bo, C., Ya-Chao, Z., Ling-Ping, H. and Xiao-Dong, W., 2019. Imaging quality evaluation of soft X-ray grazing incidence telescope. *Optics and Precision Engineering*, 27(10), pp.2136–2143.
 41. Kisoo, K., Kyung-Won, J., Jae-Kwan, R. and Ki-Hun, J., 2020. Biologically inspired ultrathin arrayed camera for high-contrast and high-resolution imaging. *Light Sci. Appl.*, 9(28), DOI: [10.1038/s41377-020-0261-8](https://doi.org/10.1038/s41377-020-0261-8).
 42. Chang, X., Bian, L. and Zhang, J., 2021. Large-scale phase retrieval. *eLight*, 1, p.4, DOI: [10.1038/s41377-020-0264-5](https://doi.org/10.1038/s41377-020-0264-5).
 43. Li, C., Wang, H., Wang, F., Li, T., Xu, M., Wang, H., Wang, Z., Zhan, X., Hu, W. and Shen, L., 2020. Ultrafast and broadband photodetectors based on a perovskite/organic bulk heterojunction for large-dynamic-range imaging. *Light Sci. Appl.*, 9, p.31, DOI: [10.1038/s41377-020-0264-5](https://doi.org/10.1038/s41377-020-0264-5).
 44. Stoev, I.D., Seelbinder, B., Erben, E., Maghelli, N. and Kreysing, M., 2021. Highly sensitive force measurements in an optically generated, harmonic hydrodynamic trap. *eLight*, 1, p.7, DOI: [10.1186/s43593-021-00007-7](https://doi.org/10.1186/s43593-021-00007-7).
 45. Wu, S., Cheng-Shan, H., Heng-Yi, L., Xu-Cheng, X. and Chang-Hong, H., 2019. Dynamic range extending method for push-broom multispectral remote sensing cameras. *Chinese Optics*, 12(4), pp.905–912.
 46. Zhao, Y., Song, B., Wang, M., Zhao, Y. and Fan, Y., 2021. Half-tone spatial frequency domain imaging enables kilohertz high-speed label-free non-contact quantitative mapping of optical properties for strongly turbid media. *Light Sci. Appl.*, 10, p.245, DOI: [10.1038/s41377-021-00681-9](https://doi.org/10.1038/s41377-021-00681-9).
 47. Cheng-Hao, L., Xu, H., Qi, J., Xiao-Hui, Z. and Ning, L., 2020. Design of high spatiotemporal resolution dynamic star simulator. *Optics and Precision Engineering*, 28(3), pp.515–525.
 48. Jin, Z., Janoschka, D., Deng, J., Ge, L., Dreher, P., Frank, B., Hu, G., Ni, J., Yang, Y., Li, J., Yu, C., Lei, D., Li, G., Xiao, S., Mei, S. and Giessen, H., Zu Heringdorf, F.M. and Qiu, C.-W., 2021. phyllotaxis-inspired nanosieves with multiplexed orbital angular momentum. *eLight*, 1, p.5, DOI: [10.1038/s41567-019-0487-7](https://doi.org/10.1038/s41567-019-0487-7).
 49. Xiong, J. and Wu, S.T., 2021. Planar liquid crystal polarization optics for augmented reality and virtual reality: From fundamentals to applications. *eLight*, 1, p.3, DOI: [10.1038/s41377-021-00567-w](https://doi.org/10.1038/s41377-021-00567-w).
 50. Rank, E.A., Sentosa, R., Harper, D.J., Salas, M., Gaugutz, A., Seyringer, D., Nevlacsil, S., Maese-Novo, A., Eggeling, M., Muellner, P., Hainberger, R., Sagmeister, M., Kraft, J., Leitgeb, R.A. and Drexler, W., 2021. Toward optical coherence tomography on a chip: In vivo three-dimensional human retinal imaging using photonic integrated circuit-based arrayed waveguide gratings. *Light Sci. Appl.*, 10(6), DOI: [10.1038/s41377-020-00450-0](https://doi.org/10.1038/s41377-020-00450-0).
 51. Chen, Z. and Segev, M., 2021. Highlighting photonics: Looking into the next decade. *eLight*, 1, p.2, DOI: [10.1186/s43593-021-00002-y](https://doi.org/10.1186/s43593-021-00002-y).
 52. Wang, D., Liu, F., Liu, T., Sun, S.L., He, Q. and Zhou, L., 2021. Efficient generation of complex vectorial optical fields with metasurfaces. *Light Sci. Appl.*, 10(67), DOI: [10.1038/s41377-021-00504-x](https://doi.org/10.1038/s41377-021-00504-x).
 53. Avola, D., Cinque, L., Fagioli, A., Foresti, G.L. and Piciarelli, C., 2021. Automatic estimation of optimal UAV flight parameters for real-time wide areas monitoring. *Multimed. Tools Appl.*, 80, pp.25009–25031.
 54. Yang, W., Wenjie, Z., Lin, W., Xuemin, L., Meng, F. and Shirui, P., 2016. *Iterative Views Agreement: An Iterative Low-Rank Based Structured Optimization Method to Multi-View Spectral Clustering*, AAAI Press.
 55. Wang, Y., Wu, L., Lin, X. and Gao, J., 2018. Multiview spectral clustering via structured low-rank matrix factorization. *IEEE Trans. Neural Networks Learn. Syst.*, 29, pp.4833–4843.
 56. Qi, P., Luo, Y., Shi, B., Li, W., Liu, D., Zheng, L., Liu, Z., Hou, Y. and Fangl, Z., 2021. Phonon scattering and exciton localization: Molding exciton flux in two dimensional disorder energy landscape. *eLight*, 1, p.6, DOI: [10.1186/s43593-021-00006-8](https://doi.org/10.1186/s43593-021-00006-8).